View Article Online
View Journal

Dalton Transactions

An international journal of inorganic chemistry

Accepted Manuscript

This article can be cited before page numbers have been issued, to do this please use: D. Giovanardi, G. Cagossi, P. Pelagatti, P. Zolotarev, P. P. Mazzeo, A. Bacchi, L. Carlucci and D. M. Proserpio, *Dalton Trans.*, 2025, DOI: 10.1039/D5DT01321F.

ROYAL SOCIETY OF CHEMISTRY

rsc.li/dalton

View Article Online
DOI: 10.1039/D5DT01321F

ARTICLE

Collapse or Capture? Guest-Induced Response of Two Structurally Distinct Pillared-MOFs upon exposure to Pyridines and Quinolines

Received 00th January 20xx,
Accepted 00th January 20xx

DOI: 10.1039/x0xx00000x

Dario Giovanardi,[a] Giorgio Cagossi,[a] Pavel N. Zolotarev,[b] Paolo P. Mazzeo,[a] Alessia Bacchi,[a] Lucia Carlucci,[b] Davide M. Proserpio,[b] and Paolo Pelagatti*[a,c]

The response of two differently entangled Zn-containing pillared Metal-Organic Frameworks (MOFs) toward quinolines and pyridines have been studied. The corresponding products have been defined by single crystal X-ray diffraction analysis, when possible through single-crystal-to-single-crystal transformations. These two MOFs have similar chemical compositions, each consisting of a dicarboxylate linker (4,4′-biphenyldicarboxylate or 2,6-naphthalenedicarboxylate) and the same bis-amide-bis-pyridine pillar. Either the flexible and interpenetrated MOF PUM168 and the rigid and polycatenated PUM210 exhibit good uptake propensity towards quinoline, although the structural modelling of the whole included guest molecules was successful only for PUM168. For PUM210 only one molecule of quinoline coordinated to a metal center was modeled, the remaining being randomly distributed along the channels. Both PUM168 and PUM210 crystals rapidly degrade once put in contact with liquid pyridines. The decomposition products of PUM210 in pyridine were structurally characterized, giving insights on the degradation pathway. This involves the replacement of the bis-amide-bis-pyridine pillar by pyridine with formation of a new homoleptic 1D-coordination polymer in which Zn ions are bound to naphthalenedicarboxylate dianions and pyridine molecules. Finally, uptake of the chelating 8-hydroxy-quinoline by PUM168 led to the protonolysis of the dicarboxylate linker and extraction of Zn ions from the framework, with formation of the bis-chelate complex Zn(8-hydroxyquinolinate)$_2$.

Introduction

Since their appearance, the use of metal organic frameworks for the inclusion of organic molecules has been a topic of interest.[1,2] The possibility to include active ingredients in a structurally well-defined material is of paramount importance for the understanding of the host-guest interactions responsible of the uptake. The advantage of using MOFs is related to their high crystallinity that makes feasible the precise description of the supramolecular organization adopted by the included guest molecules. On this approach is based the so-called crystallization sponge method,[3] where crystalline containers, such as ad-hoc tailored MOFs, are used for the ordered inclusion of guest molecules.[4,5] The final result is a crystal that can be analysed by single crystal X-ray diffraction analysis, which returns the structural characterization of the included guest even when this is a liquid or a solid reluctant to crystallization. This topic has been recently reviewed.[6] The precise knowledge of the host-guest interactions in the loaded crystal is also fundamental for the understanding and tuning of the guest release from the crystal, which is of relevance for controlled delivery of active guest compounds.

In the last years, we have described the host capacity of the mixed-ligand MOF **PUM168** (PUM: "Parma University Materials") towards a series of oxygen-containing guests.[7–9] **PUM168** is formed by Zn-paddle-wheels containing 4,4′-biphenyldicarboxylate dianions, pillared by di-isonicotinoyl linkers, hereinafter named **L1**, containing the same biphenyl scaffold (Figure 1, left). The triple interpenetrated framework originates meandered microporous channels whose sizes are compatible with the inclusion of a pool of small organic molecules. In the pristine crystals the channels are filled with molecules of DMF, some of which are hydrogen bonded to the amide groups of the framework.

Massive uptake of naturally occurring liquid phenol derivatives, such as the essential oil components eugenol, thymol and carvacrol, were observed by soaking the native crystals into the pure liquids or mixture thereof, leading to highly crystalline materials whose single-crystal X-ray diffraction analysis unveiled the structural organization adopted by the included guest molecules and the structural rearrangements undergone by the host framework.[7,9] In details, two different guest anchoring sites were recognized: the amide groups of the isonicotinoyl moiety and the carboxylate-containing paddle-wheels. In both cases, hydrogen bond interactions were responsible of the guest stabilization. The distribution of the guest molecules among the two different receptor sites was guest-dependent and mainly governed by the steric

[a] Department of Chemical Science, Life Science and Environmental Sustainability, University of Parma, Parco Area delle Scienze 17/A, 43124 Parma, Italy.
[b] Dipartimento di Chimica, Università degli studi di Milano, 20133 Milano, Italy
[c] Interuniversity Consortium of Chemical Reactivity and Catalysis (CIRCC), Via Ulpiani 27, 70126 Bari, Italy.

† Footnotes relating to the title and/or authors should appear here.
Supplementary Information available: optical and SEM images, NMR and IR spectra, TGA and PXRD traces, structural information. See DOI: 10.1039/x0xx00000x

View Article Online
DOI: 10.1039/D5DT01321F

requirements of the different included species.[9] In all cases, guest uptake triggered a structural rearrangement of the crystalline framework involving a sliding of the MOF frames, preserving crystallinity. Within this frame of research activity, we became interested to study the host-capacity of **PUM168** towards N-containing heterocycles, such as pyridines (PY) and quinolines (QUI). Although PY and QUI cannot be considered active compounds *per se*, they are used in several industrial and pharmaceutical processes, and their persistence, toxicity and potential impact on the ecosystem pose serious concerns on their use.[10–12] For these reasons, their monitoring and removal from the environment by adsorbents is desired and their inclusion in coordination polymers is documented.[13–15] However, their coordinating capability makes them potentially reactive toward the metal centre contained in the SBU, which may translate in the framework degradation. In fact, examples where the inclusion of molecules containing pyridine rings has been structurally elucidated are limited,[13,16–18] being in most of the cases derived from computational approaches.[19,20] The same remains true in the case of quinolines.[14,21] Based on these premises, we became interested in studying the effect of N-heterocyclic guests on the structure of two pillared MOFs with distinct entanglement modes, focusing either on framework flexibility or guest uptake behaviour. In addition to **PUM168**, **PUM210**[22] was considered particularly well suited to study the effect of the presence of metal nuclei easily accessible by N-heterocyclic guests. Like **PUM168**, **PUM210** combines coordination of L1 and of a dicarboxylate linker, 2,6-naphthalenedicarboxylate, to Zn(II), but displays parallel polycatenation (Figure 1, right)[23] based on two different paddle-wheel SBUs, as reported in Figure 1. One is a complete paddle-wheel, of formula $[Zn_2(COO)_4(py)_2]$, while the other is a truncated paddle-wheel of formula $[Zn_2(COO)_4(py)(H_2O)]$, where a molecule of water takes the place of a pyridine-linker. The presence of a labile coordinated solvent is expected to facilitate the binding of the guest molecule, as observed by us using a porous MOF containing Cu-paddle-wheels, after removal of a pre-coordinated water molecule.[16] Moreover, differently from **PUM168**, the polycatenated framework of **PUM210** is less dynamic, as observed during repeated manipulations, like transmetallation,[22] thermal activation[24] and inclusion of phenol derivatives.[25] The coordinative unsaturation of the SBU is then expected to promote guest binding, while flexibility is expected to promote guest inclusion.

We selected, as reported in Chart 1, a collection of N-containing heterocycles that, differently from phenols, can only function as hydrogen bond acceptors through the heteroatom, except when functionalized with proper hydrogen-bond specific groups, like in the case of 3-hydroxymethylpyridine, 4-aminomethylpyridine and 8-hydoxyquinoline. Interactions of the type N_{py}…H-N(C=O) with the amide groups installed in the MOF framework can then be envisaged. Hence, in this contribution, we describe how the crystals of **PUM168** and **PUM210** respond to a series of liquid N-containing heterocycle guests, Chart 1.

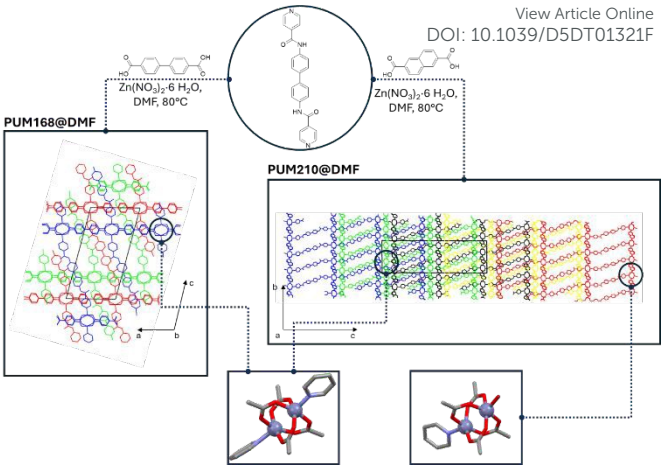

Figure 1 Representation of the synthetic paths to obtain **PUM168** (left) and **PUM210** (right), along with the different entanglements and SBUs featuring the two MOFs.

When possible, the pristine crystals (**PUM168@DMF** and **PUM210@DMF**) were soaked in the neat liquid guest, following the same protocols developed for the uptake of essential oil components.[7,9] When necessary, like in the case of 8-OH-QUI, acetonitrile solutions of the guest were used. In these cases, the crystals of **PUM168@DMF** were first converted into **PUM168@ACN**[26] prior to soaking. The guest-exchange processes were monitored by ^{1}HNMR, TGA and, whenever applicable, by single-crystal X-ray diffraction analysis. Particular attention was given to the stability of the MOF crystals towards the different guests, highlighting the guest-induced structural transformations.

Experimental

Materials and Methods.

PUM168 and **PUM210** were prepared following the reported procedure.[7,22] Pyridines (PY: pyridine, 4-acetyl pyridine, 3-hydroxymethyl pyridine and 4-aminomethyl pyridine) and quinolines (QUI: quinoline and 8-hydorxy-quinoline) were commercially available and used as received.

Soaking experiments.

The soaking experiments were conducted using crystals of **PUM168@DMF**, **PUM210@DMF** and **PUM168@ACN**. The ACN solvated crystals were used when necessary to dissolve the solid guest in the same solvent. Acetonitrile was selected since it does not damage the MOF crystals and it is able to completely remove the DMF contained in the pristine crystals, without significantly affecting the potential void of the same. The DMF/ACN exchange was conducted as previously reported,[26] at room temperature for the desired time, visually inspecting for possible crystal deterioration. Then, part of the crystals was picked up and analyzed by ^{1}HNMR, TGA and, when possible, by SC-XRD analysis.

View Article Online
DOI: 10.1039/D5DT01721F

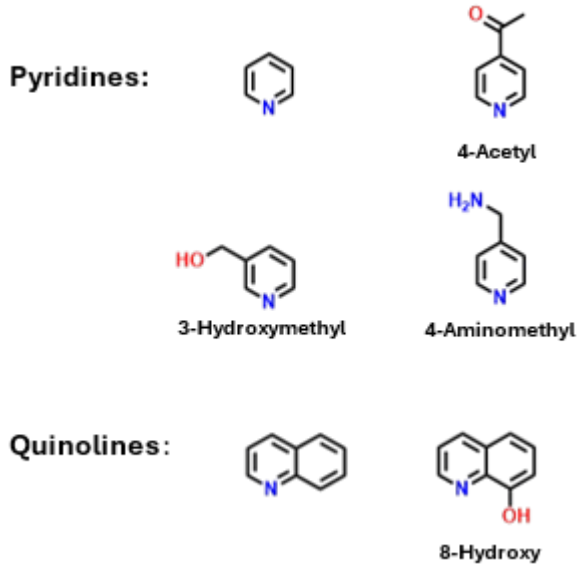

Chart 1 Structural schemes of the N-heterocyclic guests used in this work

General procedure for the preparation of the samples.

The TGA and ^{1}H NMR analyses were conducted after having gently dried the crystals over a filter paper to remove the solvent molecules covering the crystal surface. When crystal fragmentation was evident, the presence of an exclusive crystalline phase was ascertained by collecting X-ray data on crystals of different sizes.

Thermogravimetric analyses.

Thermogravimetric analyses (TGA) were performed with a PerkinElmer TGA 8000 instrument (mass sample: 2−5 mg) by means of a Pt crucible in a non-reductive atmosphere (air flux 30 mL/min) in the temperature range of 30−500 °C at 10 °C/min. Higher temperatures were not applied to avoid possible crucible damage due to the high metal content of the samples.

FT-IR spectroscopy.

FT-IR spectra were recorded by means of a PerkinElmer Spectrum Two FT-IR spectrophotometer coupled with the PerkinElmer UATR accessory and diamond crystal plate in the range of 400−4000 cm^{-1}.

^{1}H NMR Spectroscopy.

^{1}H NMR spectra were recorded on a Bruker Avance spectrometer operating for ^{1}H at 400 MHz at 25 °C after dissolution of the sample in CF_3COOD (TFA-d) and dilution in $(CD_3)_2SO$ (DMSO-d_6). Chemical shifts (δ) are expressed in ppm relative to the residual peak of deuterated DMSO (^{1}H = 2.50 ppm).

Single crystal X-ray diffraction.

Single crystal X-ray diffraction analyses of **PUM168@(quino)$_1$**, **PUM168@(quino)$_7$** were collected on a Bruker D8 Venture diffractometer equipped with a kappa goniometer, an Oxford Cryostream, and a Photon II detector using microfocused Cu Kα radiation (λ = 1.54178 Å). Crystals of **PUM210@(quino)$_1$** and **PUM210_PY** were mounted over a Bruker D8 Venture diffractometer equipped with a kappa goniometer, an Oxford Cryostream and a Photon III detector, using microfocused Mo Kα radiation (λ=0.7107 Å). Prior to being subjected to X-ray diffraction analysis, the crystals were dipped in a drop of Fomblin oil to avoid guest loss. Lorentz polarization and absorption corrections were applied for all experiments. Data reduction was carried out using APEX v5 software. Structures were all solved by direct methods using SHELXT[27] and refined by full-matrix least squares on all F^2 using SHELXL,[28] as implemented in Olex2,[29] using anisotropic thermal displacement parameters for all non-hydrogen atoms. Calculation of the unmodelled solvent electron densities were carried out applying cycles of SQUEEZE/PLATON[30] on the structures, as in **PUM210@(quino)$_1$, PUM168@(quino)$_7$** and **PUM168@(quino)$_1$**. Table 1 reports crystal data collection parameters and refinement results. The crystallographic data of **PUM168@(quino)$_1$**, **PUM168@(quino)$_7$**, **PUM210@(quino)$_1$** and **PUM210_PY** have been deposited in the CSD with CCDC code 2450670, 2450672, 2450671 and 2450669, respectively. The use of @ in the materials names indicate guest inclusion whereas the use of the underscore _ refers to the decomposition product deriving from the contact with the guest.

Table 1 Crystallographic tables for the four structures reported: **PUM168@(quino)$_7$**, **PUM168@(quino)$_1$**, **PUM210@(quino)$_1$** and **PUM210_PY**

View Article Online
DOI: 10.1039/D5DT01321F

Identification code	***PUM168@(quino)$_7$***	***PUM168@(quino)$_1$***	***PUM210@(quino)$_1$***	***PUM210_PY***
Empirical formula	$(C_{78}H_{51}O_{15}N_6Zn_3)(C_3H_7NO)(C_9H_7N)_{6.75}$	$(C_{78}H_{51}O_{15}N_6Zn_3)(C_2H_3N)_{8.5}(C_9H_7N)_{0.75}$	$(C_{84}H_{51}O_{19}N_6Zn_4)(C_9H_7N)_2(C_3H_7NO)$	$C_{37}H_{31}N_5O_4Zn$
Formula weight	2453.25	1954.18	1985.13	675.04
Temperature/K	200.00	200.00	150.00	200
Crystal system	triclinic	triclinic	triclinic	Monoclinic
Space group	P-1	P-1	P-1	P2/n
a/Å	15.2374(3)	15.0514(7)	13.1342(9)	9.7431(13)
b/Å	15.2428(3)	15.0686(8)	13.1346(8)	9.2259(10)
c/Å	27.0220(5)	26.8387(12)	31.665(2)	17.642(2)
α/°	96.3530(10)	86.567(3)	87.768(2)	90
β/°	98.1620(10)	78.620(3)	87.468(2)	98.650(13)
γ/°	90.3930(10)	60.082(3)	86.876(2)	90
Volume/Å^3	6172.8(2)	5166.9(5)	5445.6(6)	1567.7(3)
Z	2	2	2	2
ρ_{calc}g/cm^3	1.320	1.256	1.211	1.430
μ/mm^{-1}	1.261	1.365	0.936	0.833
F(000)	2540.0	2018.0	2034.0	700.0
Crystal size/mm^3	0.025 × 0.022 × 0.018	0.021 × 0.018 × 0.015	0.025 × 0.02 × 0.015	0.025 × 0.02 × 0.018
Radiation	CuKα (λ = 1.54178)	CuKα (λ = 1.54178)	MoKα (λ = 0.71073)	Mo Kα (λ = 0.71073)
2Θ range for data collection/°	5.836 to 140.132	6.726 to 141.204	3.866 to 50.054	7.3 to 51.354
Index ranges	-18 ≤ h ≤ 18, -18 ≤ k ≤ 18, -32 ≤ l ≤ 32	-18 ≤ h ≤ 18, -18 ≤ k ≤ 18, -32 ≤ l ≤ 31	-15 ≤ h ≤ 15, -12 ≤ k ≤ 15, -36 ≤ l ≤ 37	-11 ≤ h ≤ 11, -11 ≤ k ≤ 11, -21 ≤ l ≤ 21
Reflections collected	146003	100135	110594	11881
Independent reflections	23360 [R_{int} = 0.0587, R_{sigma} = 0.0337]	19665 [R_{int} = 0.0917, R_{sigma} = 0.0615]	19068 [R_{int} = 0.1175, R_{sigma} = 0.1028]	2983 [R_{int} = 0.0756, R_{sigma} = 0.0784]
Data/restraints/parameters	23360/1134/1696	19665/612/1192	19068/298/1041	2983/0/221
Goodness-of-fit on F^2	1.041	1.043	1.060	1.017
Final R indexes [I>=2σ (I)]	R_1 = 0.0789, wR_2 = 0.2335	R_1 = 0.1098, wR_2 = 0.3243	R_1 = 0.0984, wR_2 = 0.2507	R_1 = 0.0468, wR_2 = 0.0798
Final R indexes [all data]	R_1 = 0.0933, wR_2 = 0.2503	R_1 = 0.1457, wR_2 = 0.3616	R_1 = 0.1361, wR_2 = 0.2760	R_1 = 0.0806, wR_2 = 0.0885
Largest diff. peak/hole / e Å^{-3}	0.96/-0.94	1.58/-0.98	2.05/-1.15	0.32/-0.30

View Article Online
DOI: 10.1039/D5DT01215

Results and Discussion

Soaking experiments with PUM168.

The three-fold interpenetrated framework of **PUM168@DMF** contains meandered channels that represent about 50% of the total cell volume (Mercury, probe radius of 1.2Å).[7] The aperture of the channels is 7.1 x 15.1 Å^2 compatible with the inclusion of small organic molecules. In the pristine material, 12 DMF molecules fill the voids of the framework, with some of them hydrogen bonded to the amide groups of the pillar. Several O-containing guests have already been hosted in **PUM168** through soaking experiments where the initially included DMF was replaced by the incoming guest.[7,9,26] To favor the occurrence of host-guest contacts, and then the feasibility of a good uptake, in addition to pure pyridine, three liquid PY species containing hydrogen-bond active substituents, such as carbonyl (4-acetylpyridine), hydroxyl (3-hydroxymethylpyridine) or amino (4-aminomethylpyridine) groups (Chart 1) were selected. The molecular volume of the guests (pyridine = 87 Å^3, 3-hydroxymethylpyridine = 111 Å^3, 4-aminomethylpyridine = 115 Å^3, 4-acetylpyridine = 125 Å^3, and quinoline = 135 Å^3)[31] are compatible with the pore dimensions of **PUM168**, corresponding to a calculated potential void of 3059Å^3. With these species, interactions involving the pyridine nitrogen or the hydrogen-bond active functionality with the amide groups of the framework can be envisaged. Since these compounds are liquid at room temperature, the pristine crystals of **PUM168@DMF** were soaked in the neat liquids, following the same procedure adopted with essential oil components.[7,9] Optical microscopy evidenced the immediate opacification and bleaching of the crystals once put in contact with the guest (see Supporting Information, figures S1 and S2). The crystals turned out to be no longer suitable for single crystal X-ray analysis. Within 24 hours, the crystals had severely fragmented in thin plates (see Supporting Information, figure S2), which were again not suitable for structural characterization. A SEM inspection revealed profound fractures of the crystals, likely responsible of the observed crystal fragmentation (see Supporting Information, figure S19). Prolonging the soaking to several days led to pulverization of the crystals. XRPD analysis was indicative of the formation of different phases with some peaks related to the ligand **L1**. The ^{1}H NMR and TGA analysis conducted on the fragmented crystals were anyway indicative of the presence of the guest (see Supporting Information, figures S4-S6 for ^{1}HNMR, figures S12-S14 for TGA). Similar phenomena were reported in literature for the formation of 2D nanosheets starting from 3D architectures.[32] A different behaviour was observed with pure quinoline. Although a partial reduction of the crystals dimension was visible, the soaking did not lead to an excessive crystal degradation, as visualized also by SEM inspection (see Supporting Information, figure S20). Moreover, the crystals resulted suitable for structural characterization. The structural analysis evidenced that the MOF framework has practically retained its initial structure, as can be inferred from Figure 2 (left). Even the relative orientation of the amide groups of the interpenetrated frames is the same found in the pristine **PUM168@DMF**. Two frames display the amide groups in an acentric cisoidal orientation, while the third frame contains the amide groups in a transoidal orientation. The quinoline molecules have replaced most of the pristine molecules of DMF, except for one DMF hydrogen-bonded to an amide group of the centric transoidal net. The structural analysis led to the modelling of 6 molecules of quinoline sorted around the asymmetric unit as depicted in Figure 2 (right, named Q1-Q6). All have full occupancy but Q3, which displays a 0.5 occupancy. Among the included guests, only Q3 and Q4 are hydrogen bonded to the amide functions of the acentric net. The efficient packing of the quinoline molecules inside the cavities of the framework leaves only a calculated residual electron density of 85 electrons. The ^{1}HNMR spectrum of the digested crystals was indicative of seven molecules of quinoline and one molecule of DMF per asymmetric unit (see Supporting Information, figure S7). The 85 residual electrons can then be attributed to 1.25 molecules of disordered quinolines (see supporting information figure S27). In this way, a very good agreement between the number of quinoline molecules structurally determined (6.75), and the number of the same guest determined by NMR (7) turns out. As already observed with phenolic guests,[25] the TGA trace of **PUM168@(quino)$_7$** (Figure S15) shows a step-wise profile, which is in agreement with the high flexibility expected for the framework. In details, in the 30–300 °C temperature range the weight loss accounts for about 39%, perfectly in agreement with the observed amount of quinoline determined by ^{1}H NMR (36% related to the seven included molecules) and the residual molecule of DMF (with an expected value of 3%). For simplicity, this material will be referred to as **PUM168@(quino)$_7$**.

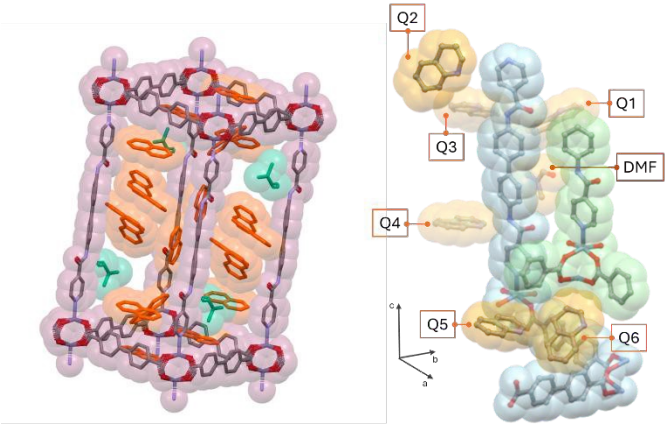

Figure 2 Left: Single cage of **PUM168@(quino)$_7$** showing the efficient packing of the quinolines in the pores. For the sake of clarity, only one out of the three interpenetrated frames is reported. Color code: quinoline orange, DMF green. Right: Distribution of the modelled quinoline molecules in **PUM168@(quino)$_7$** around the asymmetric unit of **PUM168**. The modelling of the seventh molecule of quinoline was not possible.

In the attempt to mitigate the crystal degradation observed with PYs, soaking experiments were repeated using 0.1M acetonitrile solutions of the guest. Based on our previous findings, acetonitrile is well tolerated by crystals of the MOF, and it allows for the complete removal of DMF,[26] leading to **PUM168@ACN**. Although it is known that the solvent exchange

View Article Online
DOI: 10.1039/D5DT01321F

leads to a structural deformation of the MOF framework mainly involving the 2D square nets (Figure 3 and Supporting Information, figures S30-S31),[26] the potential void of **PUM168@ACN** (2424 Å^3, 46.1% of the unit cell volume) is enough to assure the accommodation of a rather large number of guest molecules. Nevertheless, once soaked, the crystals became opaque again resulting no longer suitable for X-ray structural characterization and were no further characterized. To evaluate the effect deriving from guest concentration, crystals of **PUM168@ACN** were soaked in a 0.1 M acetonitrile solution of quinoline. The ^{1}HNMR revealed a much lower uptake, with the inclusion of only 0.75 molecules of quinoline per asymmetric unit after three days of soaking. This value did not change after prolonging the soaking up to two weeks (see Supporting Information, figure S8). Accordingly, TGA shows a weight loss of about 6.7% above 150°C, in agreement with the calculated 6% relative to the presence of 0.75 molecules of quinoline.

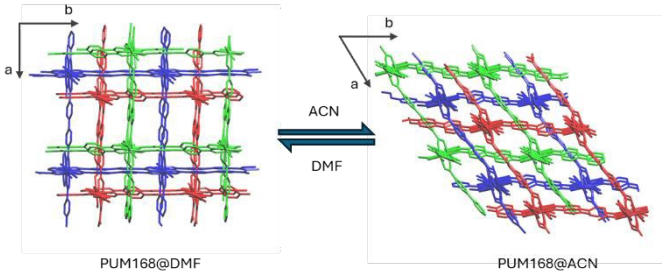

Figure 3 Representation of the two frameworks of **PUM168@DMF** (pristine) and **PUM168@ACN** (after DMF-to-ACN exchange).

The structural characterization confirmed the inclusion of one molecule of guest, displaying 0.75 chemical occupancy and, unexpectedly, positioned in the distorted squares defined by the dicarboxylate linkers (Figure 4). As for the previous inclusion product, for simplicity, this material will be referred to as **PUM168@(quino)$_1$**. The whole framework remains practically intact, without significant variations with respect to that of the starting **PUM168@ACN**, indicating that the accommodation of the guest molecule does not have any evident structural effect (see Supporting Information, figures S30-S31).

The nitrogen atom of the included quinoline is not involved in any significant intermolecular contact, the uptake being dictated by π-π stacking between quinoline and the biphenyl scaffold of the dicarboxylate linkers. The failed trapping of quinoline molecules along the framework channels is imputable to its rather high solubility in acetonitrile that allows the guest extraction from the crystal, as confirmed by the number of disordered ACN molecules distributed along the channels, as indicated by ^{1}HNMR analysis and by the unmodelled residual electron density (see Figure S28). Under these circumstances, quinoline finds a much more convenient arrangement between the thin pocket offered by the polyaromatic carboxylate squares.

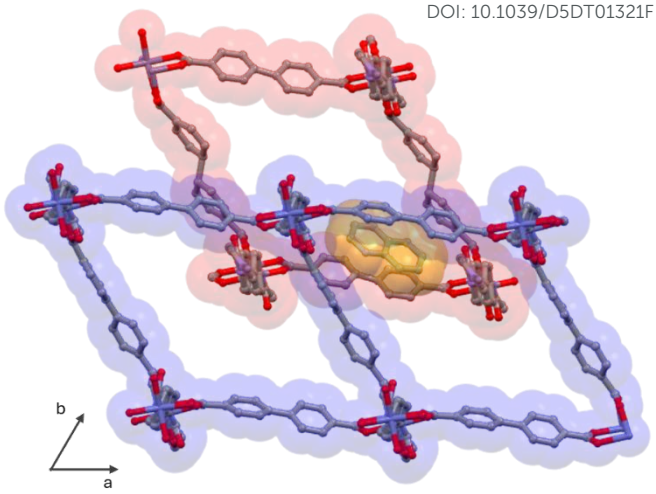

Figure 4. Visualization of the quinoline molecule (colored in yellow) trapped in the distorted squares defined by the dicarboxylate linkers in the framework of **PUM168@(quino)$_1$**.

We then became interested to study the effect of a chelating quinoline, such as 8-hydroxyquinoline (8-OH-quino).[33] This compound is solid at room temperature and then the soaking was conducted in an acetonitrile solution (0.1 M) using crystals of **PUM168@ACN**. Once soaked, the crystals became quickly opaque (Figure 5, top-left), and the solution turned light yellow. After 24 hours, small yellow crystals started to appear on the surface of the MOF crystals, as depicted in Figure 5 (top-right).

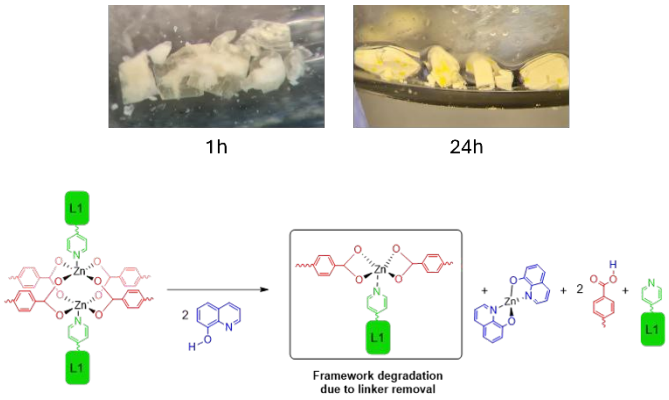

Figure 5 Top-left: Opacification of the crystals of **PUM168@ACN** after soaking in a 0.1M acetonitrile solution of 8-hydroxyquinoline. Top-right: appearance of the new crystalline phase corresponding to Zn(8-O-QUI)$_2$ on the surface of the damaged MOF crystals. Bottom: simplified reaction scheme.

After three days ^{1}H NMR and FTIR spectroscopy revealed that the yellow crystals were the bis-chelate complex Zn(8-O-quino)$_2$[34–37] (see Supporting Information, figures S10-S11). This was confirmed by a parallel reaction conducted in acetonitrile between 8-OH-quino and Zn(OAc)$_2$ in a 2:1 molar ratio. The formation of the bis-chelate complex must occur through protonolysis of one carboxylate linker promoted by two

equivalents of 8-OH-quino, with formation of one equivalent each of 4,4'-diphenyldicarboxylic acid and of the bis-chelate complex Zn(8-O-quino)$_2$, as depicted in Figure 5 (bottom). This leads to the collapse of the MOF crystal framework. The subsequent crystallization of the quinoline complex on the surface of the MOF crystals can be explained by its poor solubility in acetonitrile. The degradation process appears to involve mainly the surface of the crystal, as evidenced by the observation that cutting a damaged crystal into two parts revealed still crystalline surfaces that turned opaque if put again in contact with the solution (see Supporting Information Figure S3).

Soaking experiments with PUM210

To have insights on the effect deriving from the type of entanglement and SBU present in the framework on the guest inclusion ability of the MOF, we moved our attention on the behavior of **PUM210@DMF** towards quinoline and pyridine. This MOF is featured by polycatenated frames that contain two different SBU paddle-wheels and by a reduced dynamicity compared to **PUM168@DMF** (Figure 1, right). The facile substitution of the water molecule contained in one of the SBUs is expected to promote the uptake of the N-heterocyclic guest by coordination at the metal. As already observed with **PUM168@DMF**, also the crystals of **PUM210@DMF** bleached when soaked in neat pyridine. After five days of soaking white blocks and pale-yellow platelet crystals appeared (see supporting information, figure S2, right). EDX analysis of selected crystals evidenced that only white crystals contained Zn, (see Supporting Information, figures S21-S22).

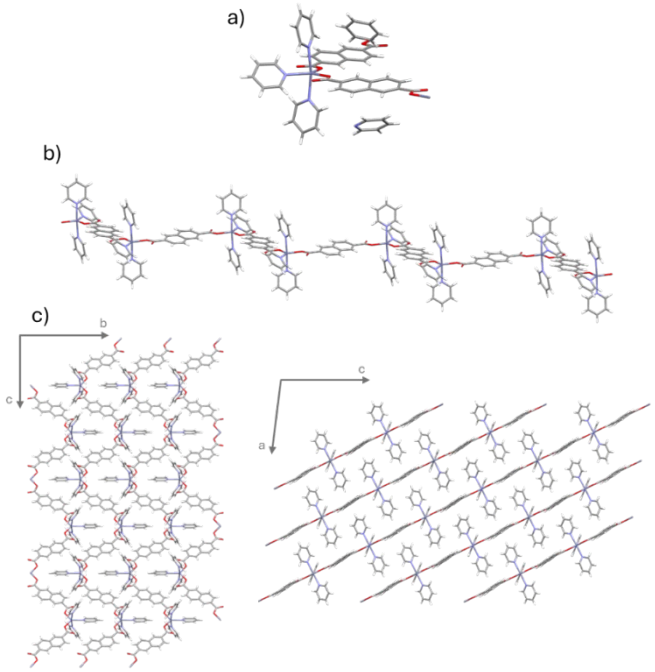

Figure 6. a) asymmetric unit of **PUM210_PY** obtained by degradation of **PUM210@DMF** in pyridine. b) Visualization of the mono dimensional chain of the polymer and c) visualization of the packing of the chains along the crystallographic axes ***a*** (left) and ***b*** (right), respectively. The included molecules of pyridine are not reported for clarity.

Single crystal X-ray analysis revealed that pale yellow crystals correspond to **L1**,[38] while white crystals are a new polymeric compound, hereinafter referred to as **PUM210_PY**, that derives from the substitution of the bis-amide pillars by pyridines, as depicted in Figure 6. **PUM210_PY** crystallizes in the monoclinic space group P2/n. Each zinc atom has a trigonal bipyramidal coordination (Figure 6a) satisfied by three pyridines and two bridging 2,6-naphthalene dicarboxylate anions to form 1D-coordination polymeric chains, as reported in Figure 6b. The 1D chains are packed to form a 3D-network held together by dispersive forces between the coordinated pyridine rings (Figure 6c). In the middle of the cavities, two molecules of pyridines were modelled. Considering the result obtained with pure pyridine, the soakings with the substituted pyridines were not carried out. The crystals of **PUM210@DMF** showed a different behaviour towards neat quinoline. Once soaked, the crystals retained their crystallinity, although a certain degree of fragmentation and opacification was visible (see supporting information figure S21). However, crystals were still suitable for single crystal X-ray analysis. The structural characterization of the new material revealed a framework very similar to that of the starting **PUM210@DMF**, but now a molecule of quinoline is coordinated to the truncated SBU in place of water (Figure 7 and 8, left).

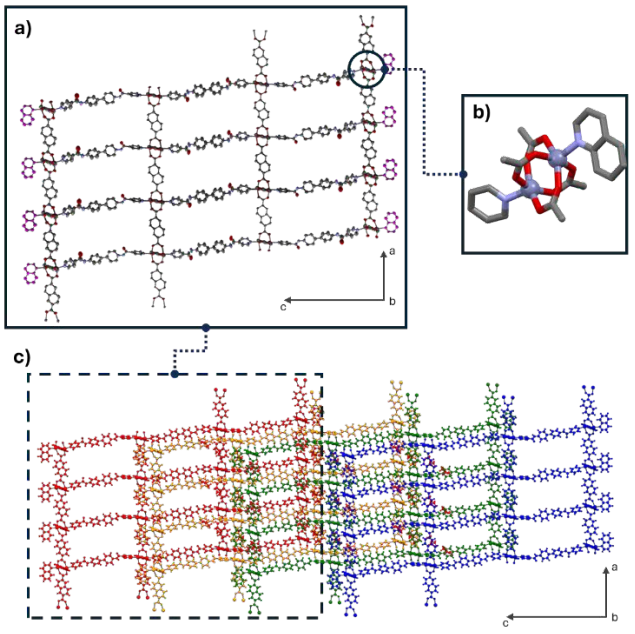

Figure 7. a) Visualization of a single frame of **PUM210@(quino)$_1$**, highlighting the coordinated quinoline in magenta. b) View of the SBU of **PUM210@(quino)$_1$** showing the coordinated molecule of quinoline occupying the apical position of the Zn atom. c) Polycatenation displayed by **PUM210@(quino)$_1$**, similar to that of the **PUM210@DMF**.[39]

This product can then be formulated as $[Zn_4(ndc)_4(\mathbf{L1})_{1.5}(QUI)]_n\cdot(DMF)_x$, hereinafter referred to as **PUM210@(quino)$_1$**. Compared to the pristine material, **PUM210@(quino)$_1$** retains the same four-fold polycatenation (Figure 7). However, it presents a different relative disposition of the amides, with the central one retaining a transoidal

View Article Online
DOI: 10.1039/D5DT01231F

arrangement while the others adopting a cisoidal orientation (Figure S32). In addition, the material retained the initial porosity (from 40% to 36% of calculated void of the unit cell volume). The disposition of the channel, however, changes. In the pristine material, the mono dimensional channel runs along the crystallographic axis ***b*** whereas in **PUM210@(quino)$_1$**, the same channel is located along the diagonal passing through the ***a,b*** plane (see Figure S33).

No molecule of quinoline could be modelled in the mono dimensional channels, while two molecules of DMF were found interacting with an amidic moiety. The application of SQUEEZE/PLATON[30] cycles calculated only 48 electrons located in the channels running along the crystallographic axis ***a*** (see supporting information Figure S29), consistent with approximatively 0.75 molecules of quinoline randomly distributed along the channels in a liquid-like configuration. The ^{1}H NMR spectrum of the digested crystals (see supporting information Figure S9) was indicative of the presence of 2.5 molecules of DMF and about 12 molecules of quinoline per asymmetric unit, data which was further confirmed by TGA analysis (see Supporting Information Figure S17). The thermal trace exhibits a two steps weight loss. The first, occurring below 150°C and not exceeding 40%, is in agreement with the release of 11 molecules of quinoline. The second, occurring in the range 150°C-300°C and corresponding to 13% weight loss, is related to the release of other 2 molecules of quinoline and 2.5 molecules of DMF anchored to the framework.

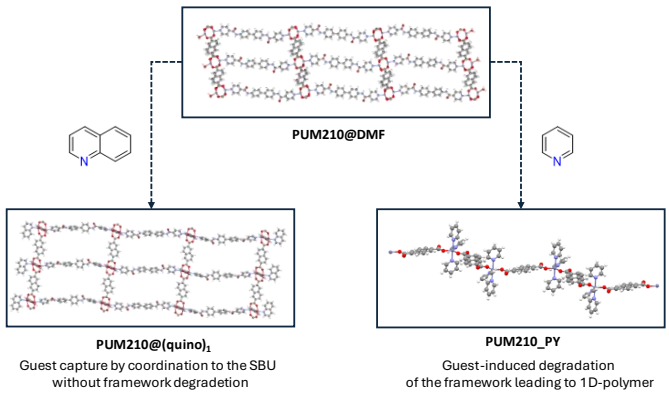

Figure 8. Different reactivity shown by **PUM210@DMF** in neat quinoline (left) and pyridine (right). In **PUM210@(quino)$_1$** the modelled DMF molecules are not reported.

Based on the results obtained with **PUM168@ACN**, soaking experiments involving 8-OH-QUI were not carried out.

Comparison of the different guest behaviour.

The soaking experiments with quinolines and pyridines were conducted under identical conditions, using a large excess of guest with respect to the few milligrams of crystals employed. Quinoline and pyridine are both good ligands for metal ions, as testified by the huge bibliography concerning their coordination chemistry.[33,36,40] The potential porosity of both microporous frameworks appears sufficient to host several molecules of the two guests. However, the behavior shown by the two guests toward the MOF crystals is markedly different. Although quinoline is sterically more demanding than pyridine, its traveling along the MOF frameworks occurs easily, as demonstrated by the massive inclusion observed with **PUM168@(quino)$_7$** (Figure 2). Moreover, quinoline can also approach the paddle-wheel SBUs contained in the frameworks, as demonstrated by its coordination trapping found with **PUM210@(quino)$_1$** (Figure 7, left). In no case, quinoline induces the displacement of **L1** and the crystals survive to soaking. A totally different behavior was observed with pyridines that, with both MOFs, revealed able to displace **L1** from the metal, as clearly demonstrated in the case of **PUM210_PY** (Figure 7, right). This behavior can be rationalized by considering that pyridine is more basic than quinoline (pKa values being 5.23 and 4.93, respectively)[41] and therefore more capable of competing for metal coordination with L1.[42] Noteworthy is the different mechanism of uptake shown by the two MOFs towards quinoline. In the flexible **PUM168**, which contain only complete paddle-wheel SBUs, quinoline molecules are hosted within the framework cavities, where they are stabilized by intermolecular contacts. In contrast, the rigid **PUM210** captures quinoline through coordination to the truncated paddle-wheel, while additional molecules are randomly distributed in the framework cavities.

Finally, protic and chelating quinolinic guests become disruptive for the MOF crystals, like observed in the case of 8-OH-QUI. In this case the framework collapses owing to protonolysis of the coordinating carboxylates, with removal of the Zn ions in the form of the bis-chelate complex Zn(8-O-QUI)$_2$.

Conclusions

In this work we compared the hosting behaviour of N-heterocylcic guests in two microporous pillared MOFs that share similar chemical composition but different entanglement. Significant guest inclusion was observed only in the case of pure quinoline, whereas the use of pyridines led to severe MOF degradation. For **PUM168@(quino)$_7$,** structural modelling of the included quinoline molecules was feasible and not limited to the molecules interacting with the amide functions of the framework. Conversely, in the case of **PUM210@(quino)$_1$**, the modelling was possible only for the molecule of quinoline coordinated to zinc atom, while the others remained disorderly distributed along the channels of the framework. The different collaborations offered by the two MOFs to the guest modelling is ascribable to their different flexibility. The known adaptive behaviour of the flexible interpenetrated **PUM168@DMF** ensures sufficiently robust host-guest interactions during the entering of the guest, allowing the guest to achieve a stable positioning within the framework. This adaptive behaviour is not present in the case of the rigid polycatenated **PUM210@DMF**, limiting the guest modelling to the coordinated quinoline. This interpretation is supported by the TGA profiles of **PUM168@(quino)$_7$** and **PUM210(quino)$_1$**. However, all the tested MOFs are unstable towards pyridines,

as evidenced by the fast degradation of their crystals. However, in the case of **PUM210@DMF** the decomposition products were unveiled by structural characterization. Here, the paddle-wheel SBUs are decomposed by replacement of the pillar **L1** with pyridines, leading to the formation of the 1D-coordination polymer **PUM210_PY**. The different tolerance shown by the two MOFs towards quinoline and pyridine cannot be associated with the different mobility of the guest through the MOF framework, but rather with their different coordination capability, where the more basic pyridine leads to a complete pillar replacement. Importantly, the use of a protic and chelating quinoline, such as 8-hydroxy-quinoline, leads again to the fast SBU degradation, triggered by protonolysis of Zn-OOC bonds with consequent removal of zinc from the MOF framework in the form of the bis-chelate complex Zn(8-O-QUI)$_2$. These findings are of paramount importance for all the researchers involved in the use of MOF crystals for the inclusion of or interaction with biologically relevant molecules, particularly given the importance that heterocycles have in biological environments.

Author contributions

D.G.: investigation, methodology, writing - original draft. G.C.: investigation; P.N.Z.: formal analysis, visualization; P.P.M.: validation; A.B.: writing - review&editing; L.C.: visualization; D.M.P.: formal analysis, visualization; P.P.: conceptualization, writing - review editing.

Conflicts of interest

"There are no conflicts to declare".

Data availability

The data supporting this article have been included as part of the Supplementary Information. Crystallographic data for **PUM168@(quino)$_7$**, **PUM168@(quino)$_1$**, **PUM210@(quino)$_1$** and **PUM210_PY** has been deposited at the CCDC under 2450670, 2450672, 2450671 and 2450669, respectively, and can be obtained from https://www.ccdc.cam.ac.uk/deposit

Acknowledgements

Chiesi Farmaceutici S.p.A. is acknowledged for the use of the Bruker D8 Venture single-crystal diffractometer. The Laboratorio di Strutturistica "M. Nardelli" of the University of Parma is acknowledged for the X-ray diffraction data collection. The Centro Interdipartimentale di Misure (CIM) of the University of Parma is thanked for instrument facilities. Dr. Ferdinando Vescovi (University of Parma) is thanked for the acquisition of SEM images. We thank Prof. Vladislav A. Blatov at the Samara Center for Theoretical Materials Science for providing the free ToposPro software (https://topospro.com).

Notes and references

1 M. D. Allendorf, M. E. Foster, F. Léonard, V. Stavila, P. L. Feng, F. P. Doty, K. Leong, E. Y. Ma, S. R. Johnston and A. A. Talin, *J. Phys. Chem. Lett.*, 2015, **6**, 1182–1195.
2 H. Vardhan, M. Yusubov and F. Verpoort, *Coord. Chem. Rev.*, 2016, **306**, 171–194.
3 Y. Inokuma, S. Yoshioka, J. Ariyoshi, T. Arai, Y. Hitora, K. Takada, S. Matsunaga, K. Rissanen and M. Fujita, *Nature*, 2013, **495**, 461–466.
4 A. D. Cardenal and T. R. Ramadhar, *ACS Cent. Sci.*, 2021, **7**, 406–414.
5 Q. Du, J. Peng, P. Wu and H. He, *TrAC - Trends Anal. Chem.*, 2018, **102**, 290–310.
6 N. Zigon, V. Duplan, N. Wada and M. Fujita, *Angew. Chemie - Int. Ed.*, 2021, **60**, 25204–25222.
7 D. Balestri, P. P. Mazzeo, C. Carraro, N. Demitri, P. Pelagatti and A. Bacchi, *Angew. Chemie Int. Ed.*, 2019, **58**, 17342–17350.
8 P. P. Mazzeo, D. Balestri, A. Bacchi and P. Pelagatti, *CrystEngComm*, 2021, **23**, 7262–7269.
9 D. Balestri, P. P. Mazzeo, R. Perrone, F. Fornari, F. Bianchi, M. Careri, A. Bacchi and P. Pelagatti, *Angew. Chemie - Int. Ed.*, 2021, 10194–10202.
10 Y. Zhang, L. Chang, N. Yan, Y. Tang, R. Liu and B. E. Rittmann, *Environ. Sci. Technol.*, 2014, **48**, 649–655.
11 Y. Bai, Q. Sun, R. Xing, D. Wen and X. Tang, *J. Hazard. Mater.*, 2010, **181**, 916–922.
12 W. Kang, Y. Cui, Y. Yang, M. Guo, Z. Zhao, X. Wang and X. Liu, *J. Hazard. Mater.*, 2021, **417**, 126160.
13 B. Tan, Z. F. Wu, M. Z. Jia, J. Zhang and G. Y. Yang, *Inorg. Chem.*, 2023, **62**, 6688–6695.
14 P. W. Seo, I. Ahmed and S. H. Jhung, *Chem. Eng. J.*, 2016, **299**, 236–243.
15 I. Ahmed, N. A. Khan, Z. Hasan and S. H. Jhung, *J. Hazard. Mater.*, 2013, **250**–**251**, 37–44.
16 D. Balestri, D. Capucci, N. Demitri, A. Bacchi and P. Pelagatti, *Materials (Basel).*, 2017, **10**, 727.
17 F. Sakurai, A. Khutia, T. Kikuchi and M. Fujita, *Chem. - A Eur. J.*, 2017, **23**, 15035–15040.
18 F. Habib, D. A. Tocher and C. J. Carmalt, *CrystEngComm*, 2023, **25**, 5001–5011.
19 Z. Hasan, M. Tong, B. K. Jung, I. Ahmed, C. Zhong and S. H. Jhung, *J. Phys. Chem. C*, 2014, **118**, 21049–21056.
20 M. J. Kim, S. M. Park, S. J. Song, J. Won, J. Y. Lee, M. Yoon, K. Kim and G. Seo, *J. Colloid Interface Sci.*, 2011, **361**, 612–617.
21 G. C. Laredo, P. M. Vega-Merino, J. Ascención Montoya-De La Fuente, R. J. Mora-Vallejo, E. Meneses-Ruiz, J. Jesús Castillo and B. Zapata-Rendón, *Fuel*, 2016, **180**, 284–291.
22 D. Balestri, I. Bassanetti, S. Canossa, C. Gazzurelli, A. Bacchi, S. Bracco, A. Comotti and P. Pelagatti, *Cryst. Growth Des.*, 2018, **18**, 6824–6832.
23 A. Delledonne, M. Orlandini, F. Terenziani, P. P. Mazzeo, A. Bacchi, L. Carlucci, A. Comotti, J. Perego and P. Pelagatti, *CrystEngComm*, 2023, **25**, 2085–2095.
24 F. Bianchi, A. Pankajakshan, F. Fornari, S. Mandal, P. Pelagatti, A. Bacchi, P. P. Mazzeo and M. Careri, *Microchem. J.*, 2020, **154**, 1–7.

View Article Online
DOI: 10.1039/D5DT01321F

25 P. Giovanardi, D.; Ribezzi, E.; Napolitano, M.; Orlandini, M.; Riboni, N.; Mazzeo, P. P.; Bacchi, A.; Bianchi, F.; Careri, M.; Pelagatti, *Chem. Eur. J.*, 2025, **31**, e202501167.

26 D. Giovanardi, P. P. Mazzeo, P. Pelagatti and A. Bacchi, *Cryst. Growth Des.*, 2023, **23**, 8726–8734.

27 G. M. Sheldrick, *Acta Crystallogr. A*, 2015, **71**, 3–8.

28 G. M. Sheldrick, *Acta Crystallogr. Sect. C Struct. Chem.*, 2008, **64**, 112.

29 O. V. Dolomanov, L. J. Bourhis, R. J. Gildea, J. A. K. Howard and H. Puschmann, *J. Appl. Crystallogr.*, 2009, **42**, 339–341.

30 A. L. Spek, *Acta Crystallogr. Sect. C Struct. Chem.*, 2015, **71**, 9–18.

31 G. B. P. Ugliengo, D. Viterbo, *J. Apll. Cryst.*, 1988, **21**, 75.

32 P. M. Chuang, P. R. Li and J. Y. Wu, *Dalt. Trans.*, 2024, **2**, 1884–1895.

33 R. Kumar, A. Thakur, Sachin, D. Chandra, A. Kumar Dhiman, P. Kumar Verma and U. Sharma, *Coord. Chem. Rev.*, 2024, 499.

34 L. L. Merritt, R. T. Cady and B. W. Mundy, *Acta Crystallogr.*, 1954, **7**, 473–476.

35 G. J. Palenik, *Acta Crystallogr.*, 1964, **17**, 687.

36 Z. F. Chen, M. Zhang, S. M. Shi, L. Huang, H. Liang and Z. Y. Zhou, *Acta Crystallogr. Sect. E Struct. Reports Online*, 2003, **59**, 814–815.

37 G. Varelas, A. Salifoglou and V. Psycharis, *Acta Crystallogr. Sect. C Cryst. Struct. Commun.*, 2013, **69**, 868–871.

38 D. Balestri, A. Bacchi, P. Scilabra and P. Pelagatti, *Inorganica Chim. Acta*, 2017, **470**, 416–122.

39 V. A. Blatov, A. P. Shevchenko and D. M. Proserpio, *Cryst. Growth Des.*, 2014, **14**, 3576–3586.

40 K. Chang, C. Huang, Y. Liu, Y. Hu, P. Chou and Y. Lin, 2004, 1731–1738.

41 M. Lõkov, S. Tshepelevitsh, A. Heering, P. G. Plieger, R. Vianello and I. Leito, *European J. Org. Chem.*, 2017, **2017**, 4475–4489.

42 R. S. Hosmane and J. F. Liebman, *Struct. Chem.*, 2009, **20**, 693–697.

Data availability statements

View Article Online
DOI: 10.1039/D5DT01321F

The data supporting this article have been included as part of the Supplementary Information.

Crystallographic data for **PUM168@(quino)$_1$**, **PUM168@(quino)$_7$**, **PUM210@(quino)$_1$** and **PUM210_PY** has been deposited at the CCDC under 2450670, 2450672, 2450671 and 2450669, respectively, and can be obtained from https://www.ccdc.cam.ac.uk/.